Red-light activation of a microtubule polymerization inhibitor via amide functionalization of the ruthenium photocage

Bretin, L.R.; Husiev, Y.; Vadde, R.; Zhang, L.; Hakkennes, M.L.A.; Abyar, S.; ... ; Bonnet, S.A.

How to cite: *Angew. Chem. Int. Ed.* **2023**, e202316425
doi.org/10.1002/anie.202316425

Photopharmacology **Hot Paper**

Red-Light Activation of a Microtubule Polymerization Inhibitor via Amide Functionalization of the Ruthenium Photocage

Ludovic Bretin[+], *Yurii Husiev*[+], *Vadde Ramu*[+], *Liyan Zhang, Matthijs Hakkennes, Selda Abyar, Andrew C. Johns, Sylvia E. Le Dévédec, Tania Betancourt, Alexander Kornienko, and Sylvestre Bonnet**

Abstract: Photoactivated chemotherapy (PACT) is a promising cancer treatment modality that kills cancer cells via photochemical uncaging of a cytotoxic drug. Most ruthenium-based photocages used for PACT are activated with blue or green light, which penetrates sub-optimally into tumor tissues. Here, we report amide functionalization as a tool to fine-tune the toxicity and excited states of a terpyridine-based ruthenium photocage. Due to conjugation of the amide group with the terpyridine π system in the excited state, the absorption of red light (630 nm) increased 8-fold, and the photosubstitution rate rose 5-fold. In vitro, red light activation triggered inhibition of tubulin polymerization, which led to apoptotic cell death both in normoxic (21 % O_2) and hypoxic (1 % O_2) cancer cells. In vivo, red light irradiation of tumor-bearing mice demonstrated significant tumor volume reduction (45 %) with improved biosafety, thereby demonstrating the clinical potential of this compound.

Introduction

Microtubules are dynamic, ATP-dependent supramolecular polymers of tubulin. They form an essential part of the cytoskeleton by providing the structure and shape of eukaryotic cells.[1] They are also involved in regulation of essential cellular processes such as cell division.[2] In consequence, microtubles are recognized as an important target for chemotherapy, as demonstrated by clinically approved tubulin-binding chemotherapeutics such as paclitaxel.[3] By blocking microtubule depolymerization, paclitaxel suppresses the dynamics of the mitotic spindle, which causes mitotic arrest and ultimately cell death.[1] Synthetic analogues of marine alkaloid rigidins have also been found cytotoxic and exert antiproliferative activities by the reverse effect, i.e., by preventing tubulin polymerization.[4–7] However, rigidins typically suffer from high hydrophobicity[8] and unselective uptake by healthy tissues, which could potentially result in side-effects in patients and limit their therapeutic potential. Both problems may be solved by a strategy called photocaging, which involves a conjugation to a photocleavable and hydrophilic group. This conjugation will improve rigidin water solubility and biologically "deactivate" them. Their high toxicity will then be recovered upon light-induced removal of the caging group in the tumor area.[8] Bicationic ruthenium photocaging groups are particularly attractive due to their ability to bind to heteroatom-containing inhibitors and their tunable photochemistry. Following platinum-based anticancer compounds, which have been used in the clinic for several decades,[9,10] ruthenium-based compounds have reached clinical trials only recently (NAMI-A, KP1019, KP1339 and TLD-1433),[11–13] and several ruthenium-based photocaged compounds are currently in pre-clinical development for photoactivated treatments of cancer.[14–17]

In the clinically approved form of anticancer phototherapy, called photodynamic therapy (PDT), a photosensitizer (PS) accumulated in the tumor is activated by visible light irradiation of the tumor, to transfer energy or electrons to dioxygen and kill cancer cells by massive production of reactive oxygen species (ROS).[18] Like in PDT, photoactivated chemotherapy (PACT) aims at sparing healthy tissues while destroying cancerous tissues efficiently. However, its mode-of-action is very different from PDT: in PACT the chemical bond between the photocaged cytotoxic inhibitor and the photocage, is cleaved by light, thereby releasing the cytotoxic agent.[8,19–22] Because such bond cleavage photoreactions are independent from the presence of dioxygen,[8,20] PACT compounds have been proposed for the treatment of hypoxic tumors, where clinically approved

[*] Dr. L. Bretin,[+] Y. Husiev,[+] Dr. V. Ramu,[+] L. Zhang, M. Hakkennes, S. Abyar, Dr. S. Bonnet
Leiden Institute of Chemistry, Leiden University, Gorlaeus Laboratories
PO Box 9502, 2300 RA Leiden (The Netherlands)
E-mail: bonnet@chem.leidenuniv.nl
A. C. Johns, Dr. T. Betancourt, Dr. A. Kornienko
Department of Chemistry and Biochemistry, Texas State University
601 University Dr., San Marcos, TX 78666 (USA)
Dr. S. E. Le Dévédec
Leiden Academic Centre for Drug Research, Leiden University, Gorlaeus Laboratories
PO Box 9502, 2300 RA Leiden (The Netherlands)
[+] These authors contributed equally to this work.

PDT agents are often ineffective.[23–25] On the other hand, several shortcomings of PACT compounds can be identified on the way to clinical applications. First, though a few ruthenium photocages have been proposed that absorb in the red or NIR region of the spectrum,[26] most of them are activated with blue or green light, which penetrates sub-optimally in biological tissues. Green light activation is currently used in clinical trial of the TLD-1433 PDT sensitizer,[27] but very few in vivo experiments have been published that directly compare the effect of green *vs.* red light activation of a photosensitive drug. Second, little biological information is available on the in vivo biological properties of ruthenium-based PACT compounds,[28] and very few animal experiment have been published to date with this type of molecular compounds.[8,29]

Results and Discussion

In this work we addressed both issues by preparing the new ruthenium-based PACT compound $[Ru^{II}(Rtpy)(bpy)(\mathbf{3})](PF_6)_2$ (**1**, Rtpy = 4′-(methylamido)-2,2′:6′,2″-terpyridine, bpy = 2,2′-bipyridine). This molecular compound releases, upon red light irradiation (625 nm), the highly cytotoxic microtubule polymerization inhibitor **3** (Figure 1).[4] In fact, **1** is an amide-functionalized derivative of the known terpyridine-based analogue $[Ru^{II}(tpy)(bpy)(\mathbf{3})](PF_6)_2$ (**4**, tpy = 2,2′:6′,2″-terpyridine), which also photoreleased the rigidin inhibitor **3** but was only tested with green light.[8] Unexpectedly, introducing a simple amide group in 4′ position of the terpyridine ligand dramatically accelerated red light activation for **1** not only in vitro but also in vivo. For the first time, the activation of **1** could be tested in vivo both with green (520 nm) and red (630 nm) light using a non-melanoma skin tumor mouse model. This experiment provided unprecedented information on the efficacy and biosafety of this type of compounds, and on the importance of the wavelength used to activate them.

1 was synthesised in 5 steps and 19 % overall yield starting from commercially available [2,2′:6′,2″-terpyridine]-4′-carboxylic acid and $[(p\text{-cymene})RuCl_2]_2$ (Figure S1). Full characterization is provided in the Supporting Information. **1** is soluble in water but its photoreactivity was studied in acetonitrile (ACN) as model solvent, as the free ligand **3** is poorly soluble in pure water and precipitates during photo-substitution experiments, which prevented quantification of the photoreactivity. In the dark, **1** was as stable in acetonitrile or OptiMEM cell-growing medium as **4** (Figures 1, S34, and S40). However, according to NMR (Figure 2; S42), UV/Vis (Figures 1; S30–37), and mass spectrometry (Figures S38–40), both green (520 nm) and red light (625 or 660 nm) irradiation of **1** in acetonitrile lead to the selective photosubstitution of the monodentate thioether ligand **3** to afford the solvate adduct $[Ru(Rtpy)(bpy)(CD_3CN)](PF_6)_2$. As suggested by Kasha's rule, for **1** the photosubstitution quantum yields (Φ) at 520 nm and 625 nm were very similar (0.0070 *vs.* 0.0074, see Table 1). The much higher molar extinction coefficient (ε) for green light

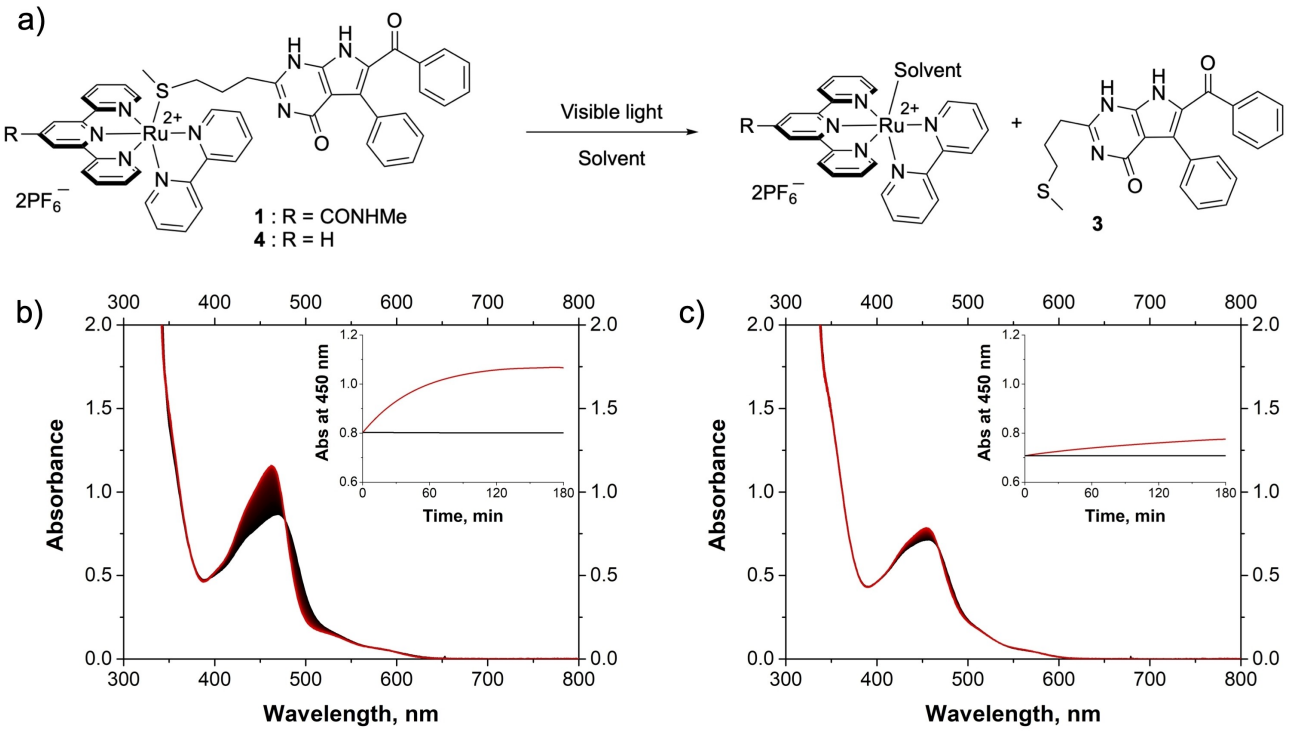

Figure 1. **a)** Formula of the ruthenium-based PACT compound **1** and release of the cytotoxic microtubule polymerization inhibitor **3** by ligand photosubstitution; **b)** Evolution of the absorption spectra of **1** in ACN (0.1 mM solution) under red light (625 nm) irradiation for 3 h at 298 K plus dark control; **c)** Evolution of the absorption spectra of reference compound **4** in ACN (0.1 mM solution) under red light (625 nm) irradiation for 3 h at 298 K plus dark control.

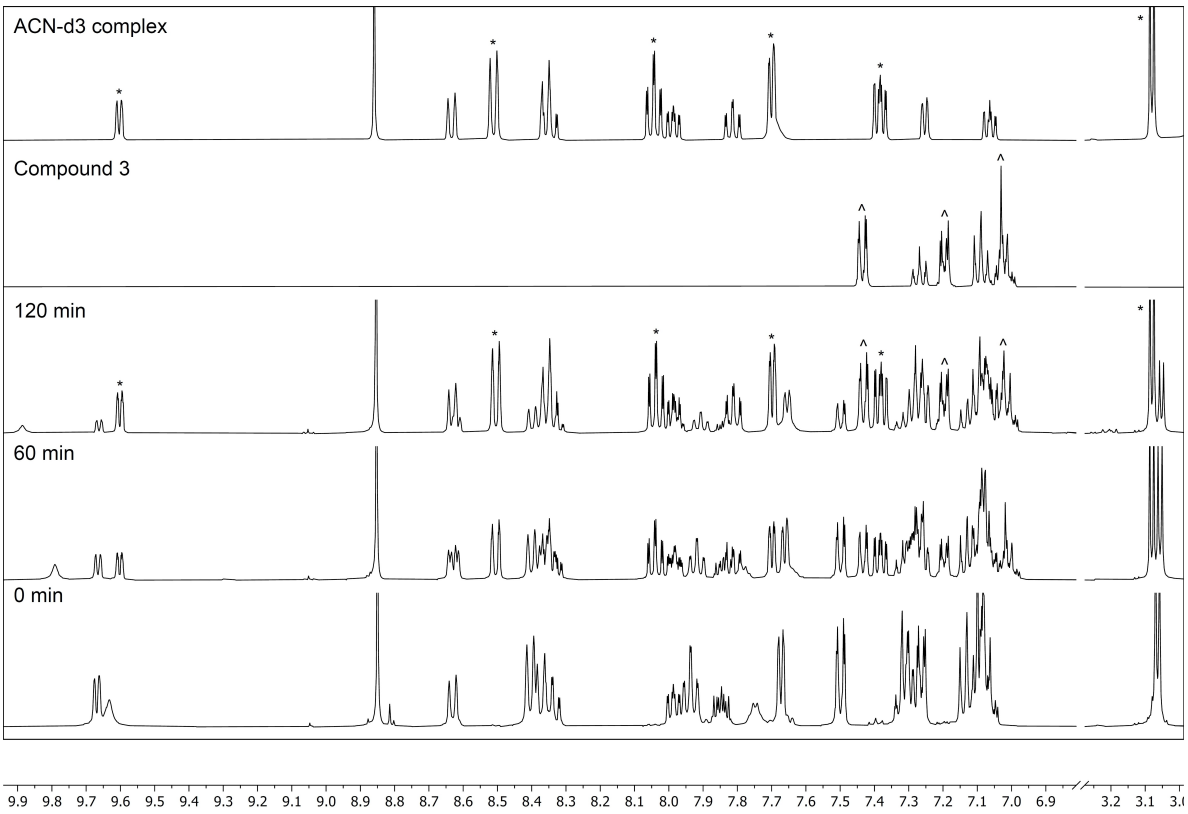

Figure 2. Evolution of ^{1}H NMR spectra of **1** in CD_3CN upon irradiation with 660 nm red light at 298 K for 2 h compared to [Ru(Rtpy)(bpy)(CD_3CN)]-$(PF_6)_2$ and **3**.

Table 1: Photochemical characterization of compounds **1** and **4** in ACN.

Compound	**1**	**4**
^{1}MLCT, nm	470	450
Φ_{520}	0.0070	0.0074
ε_{520}, $M^{-1}cm^{-1}$	1960	1510
$\varepsilon_{520}\Phi_{520}$, $M^{-1}cm^{-1}$	14	11
Φ_{625}	0.0076	0.012
ε_{625}, $M^{-1}cm^{-1}$	144	18.1
$\varepsilon_{625}\Phi_{625}$, $M^{-1}cm^{-1}$	1.1	0.22
Φ_P	0.00020	0.000030
$\Phi_\Delta(^1O_2)$	0.007	0.006

($1960\ M^{-1}cm^{-1}$), compared with red light ($144\ M^{-1}.cm^{-1}$), resulted in a higher photoreactivity ($\varepsilon\Phi$) value, hence a >10 times faster photosubstitution reaction with green light, compared with red light ($\varepsilon_{520}\Phi_{520}=14$ vs. $\varepsilon_{625}\Phi_{625}=1.1\ M^{-1}cm^{-1}$). On the other hand, **1** absorbed red light 8 times better compared with the unsubstituted compound **4** ($\varepsilon_{625}=18.1\ M^{-1}cm^{-1}$), which resulted in a red light photoreactivity that was enhanced by a factor 5 for **1**, compared with **4** ($\varepsilon_{625}\Phi_{625}=0.22\ M^{-1}cm^{-1}$, Figure 1c). Such enhancement is specific for red light, as for green light the similar quantum yields, and molar absorption coefficient resulted in similar photoreactivity for **1** and **4** (14 *vs.* $11\ M^{-1}cm^{-1}$). Finally, phosphorescence (Table S1, Figure S44) and singlet oxygen generation quantum yields (Table S2, Figures S45–47) were very low both for **1** and its photosubstitution products, which is typical for PACT compounds. All photochemical data for **1** and **4** are summarised in Table 1.

To understand the effects of the amide group on the excited states of **1**, DFT and TDDFT studies were realized for **1** and **4** using the ADF software[30] at the PBE0/TZP/COSMO level of theory in water.[31–34] Dispersion effects were corrected for by Grimme's D3 correction with BJ damping[35] and relativistic effects were scalarly corrected by ZORA[36] (Table S3). In the minimized structure of the ground state of **1** (^{1}GS, Figure 3), the dihedral angle between the average plane of the amide group and the average plane of the central pyridine ring of the terpyridine ligand was 25.1°. A similar non-zero dihedral angle (24.2°) was observed in the ^{3}MC state, which was characterized by elongated Ru–S and Ru–N_{trans} bond lengths. Strickingly, the ^{3}MLCT state, which was obtained by geometry optimization on the triplet hypersurface starting from the singlet ^{1}GS geometry, was characterized by an almost co-planar amide and terpyridine planes (dihedral angle $=-0.4°$). In the ^{3}MLCT excited state the electron originating from the metal t_{2g} orbitals, is known to localize in the π^* orbital of the terpyridine chelate; in presence of the amide group, this terpyridine-based π^* orbital was stabilized by conjugation with the carbonyl group, which stabilized the ^{3}MLCT state. As a result, the energy gap between the ^{3}MLCT and ^{3}MC states, which was $+12\ kJ.mol^{-1}$ for **4**, was increased to

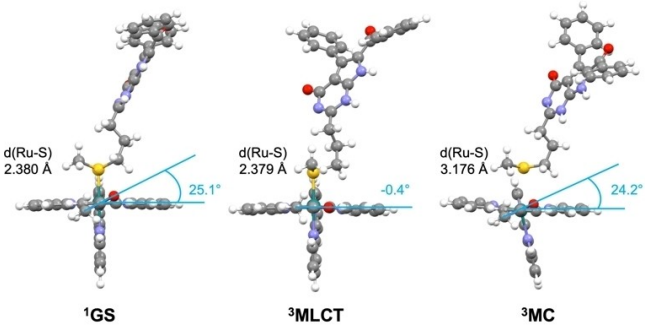

Figure 3. DFT-minimized geometry of **1** in the ground state (^{1}GS), ^{3}MLCT, and ^{3}MC excited states (PBE0/TZP/COSMO in water). The Ru–S bond lengths and dihedral angles between the amide and central pyridine planes of the terpyridine ligand are also shown.

24 kJ.mol^{-1} in **1**. Such higher energy gap was consistent with the (slightly) higher phosphorescence in **1**, compared with **4** —though both molecules are overall poorly emissive. The ^{3}MLCT stabilization had no consequence on the green light photosubstitution quantum yield Φ_{520}, but slightly decreased Φ_{625}.[37] More importantly, the lowest-energy ^{1}MLCT transitions, calculated by TDDFT on the ground state geometry, was red-shifted for **1** (471.1 nm) compared to **4** (449.1 nm), which explained the 8 times higher molar extinction coefficient of **1** observed experimentally at 625 nm, compared to **4** (Table 1). Overall, 4′-methylamide substitution of the terpyridine in **1** led to exquisite fine-tuning of the excited states of the ruthenium cage complex, which was particularly advantageous for PACT as it increased the rate of red light activation, compared with **4**, to achieve values that were compatible with in vitro and in vivo experiments.

To investigate the ability of **1** to interact with its biological microtubule target, a fluorescence-based tubulin polymerization assay was used to compare the effects of **1** (25 μM) on tubulin polymerization properties in the dark or after activation with red light (Figure 4a). In this assay, tubulin polymerization leads to a marked increase in the fluorescence intensity of the probe, as observed in presence of paclitaxel, a known tubulin polymerization enhancer. In the presence of **1** left in the dark, tubulin polymerization took place at a rate similar to the vehicle control, suggesting that non-activated **1** did not inhibit microtubule polymerization. However, upon red light activation **1** completely blocked tubulin polymerization, in a similar manner to colchicine. Therefore, photoactivation of **1** with red light clearly recovered the inhibiting properties of ligand **3**. In order to validate the inhibition properties of **1** on tubulin polymerization in vitro, immunofluorescent staining was performed in A431 non-melanoma skin cancer cells. The cells were treated with **1** (10 μM) and either irradiated with red light (630 nm, 32 J/cm^2) or left in the dark, then fixed, stained with α-tubulin 4 h after light activation, and finally imaged with a confocal microscope. As shown in Figure 4b, cells treated with **1** but kept in the dark showed a very well-established tubulin network (green filaments). In contrast, cells treated with **1** and irradiated with red light showed a complete disruption of the tubulin network and crystallization of tubulin (green dots). Altogether, both assays demonstrated that the ruthenium-caged inhibitor **1** is not functional when kept in the dark, but becomes functional upon red light irradiation, which releases free inhibitor **3**.

To further investigate the consequences on cell survival of tubulin polymerization inhibition, the phototoxic properties of **1** were studied in human skin melanoma (A375) and non-melanoma (A431) cancer cell lines. A comparison between green light irradiation, which is typically used for the activation of **4**,[8] and red light activation,[38] which is strongly accelerated for **1**, was realized, in order to evaluate the potential benefit of amide functionalization. **3** is a reported cytotoxic agent in these cell lines, but the caging aqua compound [Ru(Rtpy)(bpy)(OH$_2$)](PF$_6$)$_2$ (R=CONHMe, **2**) was also included in this study to check whether phototoxicity would originate only from ligand **3** or also from the ruthenium-containing photoproduct **2**. The 50 % effective concentration (EC$_{50}$) for cell growth inhibition was determined using 24 h drug-to-light interval, green (520 nm)

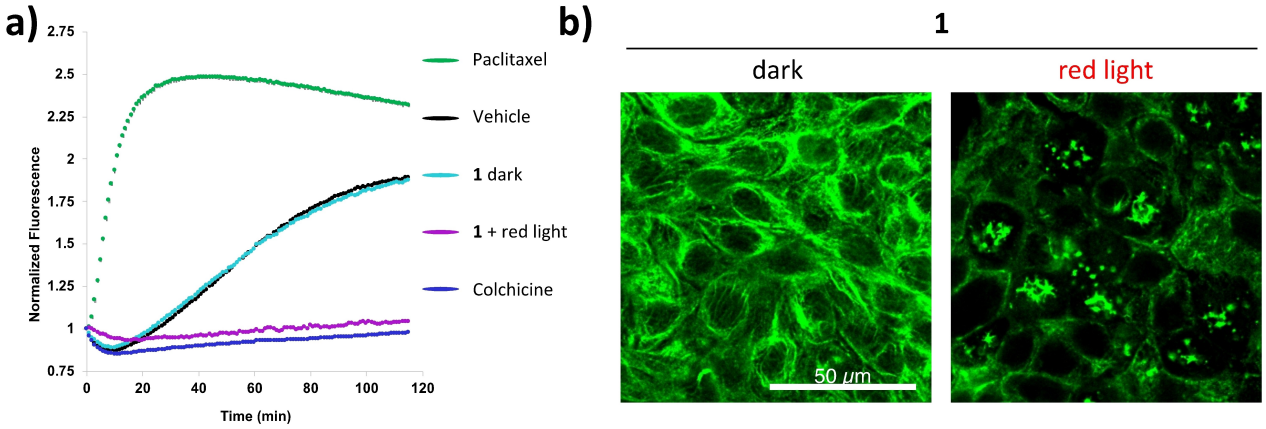

Figure 4. Red light activation of **1** shows destabilization of the microtubule network. **a)** Tubulin polymerization assay of **1** (25 μM) kept in the dark vs. after red light activation. Raw fluorescence was normalized by initial fluorescence for each sample. Paclitaxel (3 μM) was used as a tubulin polymerization enhancer and colchicine (6 μM) as a tubulin polymerization inhibitor. **b)** Confocal microscope images of A431 skin cancer cells treated with **1** (10 μM) and kept in the dark or irradiated with red light (630 nm, 32 J/cm^2), followed (4 h after light activation) by α-tubulin staining.

or red (630 nm) light, the same 32 J/cm^2 light dose, 48 h dark incubation after light activation, and a standard sulforhodamine B (SRB) assay for end-point quantification of cell viability (Table 2, Table S5).[39]

Under normoxic conditions (21 % O_2, Table 2), **1** showed similar EC_{50} in A431 and A375 cells after red light (0.8 and 1.5 μM, respectively) and green light (1.0 and 1.3 μM, respectively) activation. The deeper tissue penetration of red light does not apply in vitro using two-dimensional monolayer cell culture, where there should be no difference of light penetration between red and green light. These data suggest that the light dose of 32 J/cm^2 is high enough, even considering the difference in photochemical reactivity (εΦ) between both wavelenths, to fully activate the compound. In addition, they clearly demonstrate that **1** is highly photoactive under red light irradiation, as the photoindex ($PI=EC_{50,D}/EC_{50,L}$) is significant (71 for A431 cells and 28 for A375 cells). More interestingly, in hypoxic conditions (1 % O_2, Table 2), **1** showed similar phototoxicity after red or green light irradiation, compared to normoxic conditions, characterized by $EC_{50,\,light}$ values between 1.0 and 2.3 μM for both cell lines. The higher dark $EC_{50,D}$ values under hypoxia, compared to normoxia, are probably the result of the known resistance of hypoxic cancer cells to chemotherapy.[40,41] They led to even higher PI values under green light activation for both cell lines, compared with normoxia, while under red light irradiation PI values were comparable in hypoxia and normoxia. Altogether, these in vitro results highlight the O_2-independence of the photosubstitution reaction occurring in **1**, which was observed before.[42] Importantly, **2** was found non-toxic to both cell lines either in the dark or upon red light irradiation and in both oxygen conditions ($EC_{50} > 50$ μM, Table S5), proving that the phototoxicity observed for **1** was due mostly to the intracellular release of the cytotoxic inhibitor **3**. The morphology of treated A375 cells 24 h post-irradiation showed cell shrinkage, loss of cell-cell adherence, and blebbing of the cell membrane (Figure S51), suggesting apoptotic cell death. In addition, **1** was also evaluated in A375 3D tumor spheroids to better mimic the conditions found in 3D tumor tissues. **1** after red light irradiation showed similar phototoxicity behavior in both normoxic and hypoxic conditions with EC_{50} values of 9.5 and 15 μM, respectively (Figure S52, Table S6). Representative images demonstrated that the 3D tumor spheroids were smaller and less dense after red light irradiation, suggesting tumor cell death by **1**. Also in 3D, these in vitro data support the fact that photosubstitution of **1** is non-oxygen dependent as the phototoxicity is similar in both normoxic and hypoxic conditions.

To better understand the difference between **1** and **4** in a biological context, the photocytotoxicity of both compounds was analyzed after red and green light activation in A431 cells. As described above, **1** showed similar EC_{50} after red and green light activation. In contrast, at the same light dose **4** showed a 5-fold lower photocytotoxicity after red light activation (EC_{50} 2.5 μM) compared to green light activation (EC_{50} 0.5 μM, Figure 5a and b). This result suggested that in absence of methylamide substituent on the terpyridine the red light reaction was too slow to reach completion. This hypothesis was confirmed by a flow cytometry cell death experiment using an apoptosis/necrosis assay. A431 normoxic cells were dark treated with vehicle control, **1** (2 μM), **4** (1 μM), or cisplatin (5 μM) for 24 h, then either kept in the dark or irradiated with green ($\lambda_{irr}=520$ nm, 32 J/cm^2) or red light ($\lambda_{irr}=630$ nm, 32 J/cm^2) and further incubated in the dark for 24 h, and finally double-stained with a necrosis probe (Nuclear Green DCS1) and an apoptosis probe (Apopxin Deep Red) and analyzed by FACS (Figure 5c and S53). In this analysis, cells in the upper left quadrant "R1" represents the percentage of necrotic cells (Apop-/DCS1+), the upper right quadrant "R2" that of late apoptotic cells (Apop+/DCS1+), the lower right quadrant "R3" that of early apoptotic cells (Apop+/DCS1−) and the lower left quadrant "R4" that of alive cells (Apop-/DCS1−). For **1** the percentage of apoptotic cells was similar after green and red light activation, 41 % and 39 %, respectively (Figure 5d). For **4**, however, only 12 % of apoptotic cells were found after red light activation, vs. 10 % for vehicle control and 27 % for green light. According to this assay, **1** clearly triggered apoptotic cell death upon red light activation, while **4** could

Table 2: EC_{50} data for **1** on A431 and A375 skin cancer cell lines in the dark (D), after red- or green light irradiation, under normoxia (21 % O_2) or hypoxia (1 % O_2).

		1							
Cell line	% O_2	$EC_{50,D}$[a] (μM)	CI[b] 95 % (μM)	$EC_{50,RL}$ (μM)	CI 95 % (μM)	PI[c]	$EC_{50,GL}$ (μM)	CI 95 % (μM)	PI
A431	21	57	+17 −11	0.8	+0.3 −0.2	71	1.0	+0.4 −0.3	56
	1	77	+6.7 −6.5	2.0	+0.4 −0.4	38	1.0	+0.3 −0.2	80
A375	21	42	+8.2 −6.4	1.5	+0.6 −0.4	28	1.3	+0.5 −0.4	31
	1	>200	/	2.3	+0.9 −0.6	>88	1.0	+0.4 −0.3	>205

[a] RL: $\lambda_{irr}=630$ nm; GL: $\lambda_{irr}=520$ nm; Light dose = 32 J/cm^2; Drug-to-light interval (DLI) = 24 h. [b] 95 % confidence intervals. [c] Photoindex (PI) calculated as $PI=EC_{50,D}/EC_{50,RL\text{ or }GL}$. Data are shown based on three biologically independent experiments.

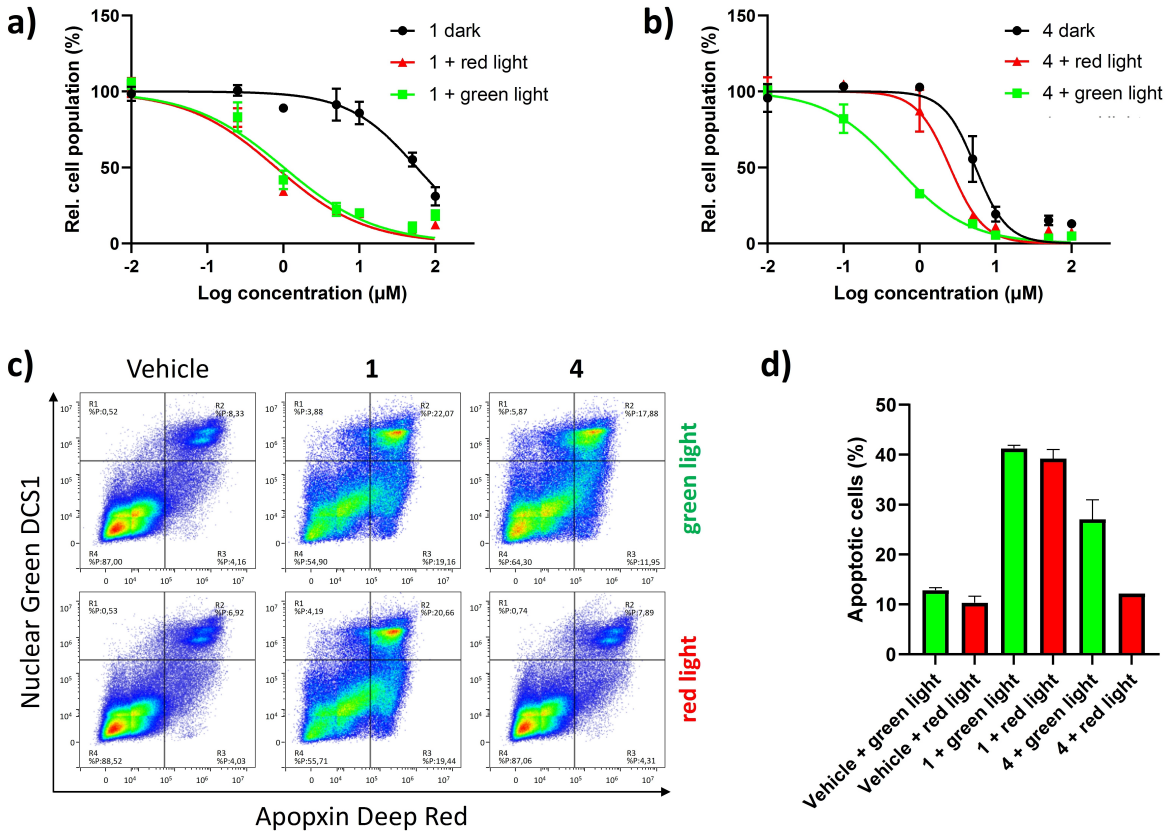

Figure 5. Phototoxicity comparison between **1** and **4** after red or green light irradiation at identical light doses. Cell viability curves and EC_{50} data for **1** (a) and **4** (b) in A431 cells kept in the dark (D), activated by red or green light. c) Cell death analysis by flow cytometry for A431 cells treated with vehicle control, **1** (2 μM), **4** (1 μM), or cisplatin (5 μM) for 24 h, then kept in the dark or activated by green or red light, further incubated for 24 h, then doubly stained with Apopxin Deep Red (apoptosis, X-axis) and Nuclear Green DCS1 (necrosis, Y-axis). R1 represents Apop-/DCS1+, R2 Apop+/DCS1+, R3 Apop+/DCS1-, and R4 Apop-/DCS1-. d) Flow cytometry quantification of the percentage of apoptotic cells for each condition (R2+R3 quadrants). Conditions: normoxia (21 % O_2), red light = 630 nm, 32 J/cm^2; green light = 520 nm, 32 J/cm^2. Data are expressed as the mean ± standard error of the mean (SEM).

not. Altogether these data highlight the fact that **1** is a better candidate for preclinical analysis in mice models as it can also be activated by red light, which is used in the clinic.

Next to preventing interaction of hydrophobic organic inhibitors such as **3** (log $P > +4$)[8] with the protein target, ruthenium-based photocaging groups often improve their water solubility. Indeed, the octanol/water partition coefficient value (log P) of **1** and **2** were much lower (+0.116 and +0.095, respectively, Table S7), demonstrating that **1** was much more water-soluble than **3** due to the water solubility of the caging group **2**. The cellular ruthenium uptake of **1** was quantified by inductively coupled plasma mass spectrometry (ICP-MS). A431 and A375 cells were treated with **1** (20 μM) for 2 h in both normoxic and hypoxic conditions, before nitric acid digestion and ruthenium concentration ICP-MS measurements (Table S8). Overall, **1** was taken up by both cell lines, with a higher cellular uptake in normoxia (34.6 ± 1.3 and 28.2 ± 3.1 μg Ru/million cells for A431 and A375 cells, respectively) than in hypoxia (25.2 ± 3.3 and 19.5 ± 3.7 μg Ru/million cells for A431 and A375 cells, respectively). On the other hand, when comparing the phototoxicity of **1** in A431 cells that had been washed with drug-free medium before red light activation, to that in A431 cells that had *not* been washed with drug-free medium before activation, we obtained much higher $EC_{50,RL}$ values in the former case (Figure S55 and Table S9). This was different from cisplatin, for which the same comparison led to essentially identical EC_{50} values for both protocols. According to this experiment, cellular uptake is slower for **1** than for cisplatin, and in our standard in vitro cytotoxicity protocol, where cells are not washed before light activation, a majority of the ruthenium molecules are photoactivated outside the cell at 24 h, before the photoreleased inhibitor **3** is taken up intracellularly to block microtubule polymerization in the follow-up 48 h dark incubation. Finally, when A375 cells were co-treated with **1** and classical endocytosis inhibitors (NaN_3, NH_4Cl and Dynasore), the cellular uptake of **1** was clearly inhibited by a factor ≈3, suggesting that **1** entered A375 cells via energy-dependent and dynamin-dependent endocytosis pathways (Figure S54).[43] These results highlighted the ability of ruthenium-based photocaging groups to solubilize in water hydrophobic organic inhibitors, while the resulting conjugate **1**, which ended up to be amphiphilic, may aggregate into nanostructures taken up at least partly by endocytosis.

Considering the good performance of **1** in vitro and its sensitivity to red light it was a perfect candidate for in vivo evaluation. For such evaluation, we decided to use human epidermoid carcinoma cells (A431) subcutaneous tumor xenografts in BALB/c nude mice, as the PI values in vitro were higher in this cell line. The experiment was designed not only to test the antitumor efficacy and biosafety of **1**, but also to investigate the difference in light activation between red light and green light, which has been often discussed but not often experimentally tested. Each mouse bore two tumors, one on each flank: the left one served as dark control, and the right one was illuminated with either green (520 nm) or red (630 nm) light at the same light dose (75 J/cm^2), to activate **1**. As a note, the chosen light dose was ca. twice as high as that used in our first in vivo experiments on compound **4** using green light (38 J/cm^2),[8] as we hope to increase tumor response. It was also ca.twice as high asthe light dose used in vitro (Table 2), since light penetration is not an issue in 2D cell monolayers while it is a known challenge for light activation in vivo. After the tumors had reached an average volume of ca.100 mm^3, mice were separated into 4 groups (7 mice per group) receiving vehicle + green light, **1** + green light, vehicle + red light and **1** + red light. Vehicle (PBS/1 % DMSO) and **1** (4 mg/kg) were administered intraperitoneally and allowed to distribute during a DLI of 30 min. Afterward, the right back flank tumor was illuminated at a wavelength-independent fluence, keeping the other tumor non-irradiated. The volume of both tumors and the body weight of each mouse were recorded 3 times a week (Figure 6a). Over a period of 30 days after compound injection, the **1** + red light group displayed a statistically significant antitumor efficacy, compared to the 3 other groups either treated with **1** but kept in the dark (−45 %, p = 0.0011), or treated with vehicle and kept in the dark (−46 %, p = 0.0002) or irradiated with red light (p = 0.0007). Representative images illustrating tumor growth between groups at the end of the study are shown in Figure 6b. Interestingly, the group treated with **1** and activated with green light showed also a significant decrease in tumor growth compared to the group treated with **1** but kept in the dark (−41 %, p = 0.0122) or to the vehicle groups (vehicle dark −39 %, p = 0.0003 and vehicle + green light −37 %, p = 0.0015, Figure 6c). However, despite the general idea of the deeper penetration of red light in biological tissues, the group **1** + red light did not show significant difference with the group **1** + green light (p = 0.8258, Figure S56). We interpret this effect as caused by the higher molar absorption coefficient of **1** at 520 nm compared with 630 nm: green light penetrates less well in tissue but is better absorbed by the compound, while red light penetrates better but is less well absorbed, which overall leads to similar antitumor effects.

Importantly, the mice showed constant body weight over 30 days, suggesting a low systemic toxicity of **1** at 4 mg/kg compound dose, also after light activation (Figure 6d). Relative to the known compound **4**, which showed significant toxicity issues at 2 mg/kg and a lower antitumor effect (−30 %) at 1 mg/kg using a DLI of 24 h and a light dose of 38 J/cm^2,[5] **1** seems to be better tolerated, while demonstrating a stronger antitumor efficacy.

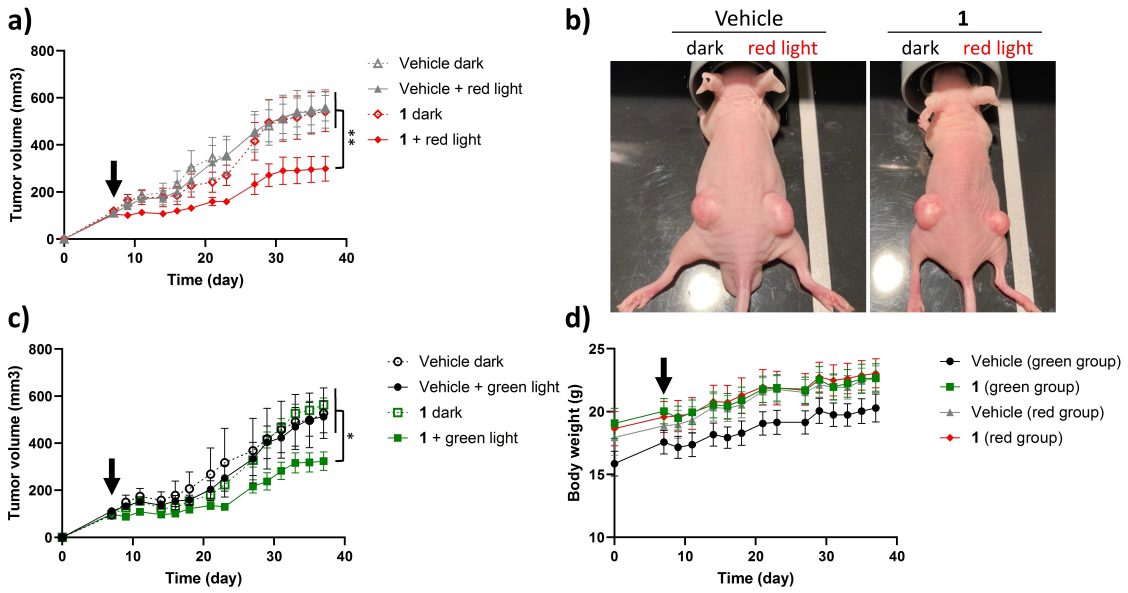

Figure 6. In vivo evaluation of ruthenium-based PACT compound **1** activated by green or red light in a subcutaneous A431 non-melanoma skin tumor mice model. a)-c) Relative tumor growth curves of A431 tumor-bearing mice treated with vehicle control (PBS/1 % DMSO) or **1** (4 mg/kg, i. p.) with or without red light activation (630 nm, a) or green light activation (520 nm, c) at a common light dose of 75 J/cm^2 and with a drug-to-light interval (DLI) of 30 min. b) Representative images illustrating tumor growth for red light-treated mouse between groups at the end of the study (30 days). d) Time evolution of the body weight of mice in the different groups. The black arrow shows compound injection. Data are expressed as the mean ± standard error of the mean (SEM). Statistical significance was evaluated by a one-way ANOVA and the Tukey's Honest Significant Difference post-hoc test and expressed as: * $p < 0.05$ and ** $p < 0.01$.

Conclusion

In summary, we have demonstrated that functionalization of **4** with a methylamide group in the 4′ position of the terpyridine ligand, resulted in a compound (**1**) with exquisitely fine-tuned excited states, characterized by improved (8x) red light absorption. This effect accelerated by a factor of 5 the red-light activation of **1** to a regime where in vitro and in vivo activation became possible, while **4** was limited to green light activation. Such modification is essential for phototherapy as red light (630 nm) is used clinically for activating FDA-approved PDT compounds (Photofrin) and can be obtained with clinical-grade red lasers. In spite of the much lower molar absorption coefficient of **1** at 630 nm, compared with 520 nm, in A431 tumor-bearing mice the tumor volume reduction was significant (45 %) upon red light irradiation of **1** at 4 mg/kg i.p. compared with vehicle control, and statistically identical with that obtained upon green light activation at the same light dose (75 J/cm^2). Importantly, the 4′-methylamide substituent also improved the biosafety of **1** compared with **4**, leading to lower toxicity of the prodrug in the dark, both in vitro and in vivo. Overall, these data demonstrate for the first time the in vivo potential of red-light activated, ruthenium-based PACT molecular compounds for the treatment of cancer.

Acknowledgements

Dr. Sipend Zheng and Hans van den Elst are kindly acknowledged for performing ESI-MS, HPLC and HRMS measurements. The Dutch Organization for Scientific Research (NWO) is kindly acknowledged for a VICI grant to S.B. European Research Council (ERC) is kindly acknowledged for a Proof-of-Concept grant to S.B. A.K. is grateful to the Denise M. Trauth Endowed Presidential Research Professorship.

Conflict of Interest

The authors declare no conflict of interest.

Data Availability Statement

The data that support the findings of this study are available in the supplementary material of this article.

Keywords: Hypoxia · Microtubule · Photocaging · Photopharmacology · Ruthenium

[1] A. L. Parker, M. Kavallaris, J. A. McCarroll, *Front. Oncol.* **2014**, *4*, https://doi.org/10.3389/fonc.2014.00153.
[2] G. J. Brouhard, L. M. Rice, *Nat. Rev. Mol. Cell Biol.* **2018**, *19*, 451–463.
[3] S. Khwaja, K. Kumar, R. Das, A. S. Negi, *Bioorg. Chem.* **2021**, *116*, 105320.
[4] D. C. Medellin, Q. Zhou, R. Scott, R. M. Hill, S. K. Frail, R. Dasari, S. J. Ontiveros, S. C. Pelly, W. A. L. van Otterlo, T. Betancourt, C. B. Shuster, E. Hamel, R. Bai, D. V. LaBarbera, S. Rogelj, L. V. Frolova, A. Kornienko, *J. Med. Chem.* **2016**, *59*, 480–485.
[5] L. V. Frolova, I. V. Magedov, A. E. Romero, M. Karki, I. Otero, K. Hayden, N. M. Evdokimov, L. M. Y. Banuls, S. K. Rastogi, W. R. Smith, S.-L. Lu, R. Kiss, C. B. Shuster, E. Hamel, T. Betancourt, S. Rogelj, A. Kornienko, *J. Med. Chem.* **2013**, *56*, 6886–6900.
[6] R. Scott, M. Karki, M. R. Reisenauer, R. Rodrigues, R. Dasari, W. R. Smith, S. C. Pelly, W. A. L. van Otterlo, C. B. Shuster, S. Rogelj, I. V. Magedov, L. V. Frolova, A. Kornienko, *ChemMedChem* **2014**, *9*, 1428–1435.
[7] R. Dasari, A. Kornienko, *Chem. Heterocycl. Compd.* **2014**, *50*, 139–144.
[8] V. H. S. van Rixel, V. Ramu, A. B. Auyeung, N. Beztsinna, D. Y. Leger, L. N. Lameijer, S. T. Hilt, S. E. Le Dévédec, T. Yildiz, T. Betancourt, M. B. Gildner, T. W. Hudnall, V. Sol, B. Liagre, A. Kornienko, S. Bonnet, *J. Am. Chem. Soc.* **2019**, *141*, 18444–18454.
[9] U. Ndagi, N. Mhlongo, M. Soliman, *Drug Des. Dev. Ther.* **2017**, *11*, 599–616.
[10] T. C. Johnstone, K. Suntharalingam, S. J. Lippard, *Chem. Rev.* **2016**, *116*, 3436–3486.
[11] S. Leijen, S. A. Burgers, P. Baas, D. Pluim, M. Tibben, E. Van Werkhoven, E. Alessio, G. Sava, J. H. Beijnen, J. H. M. Schellens, *Invest. New Drugs* **2015**, *33*, 201–214.
[12] C. G. Hartinger, M. A. Jakupec, S. Zorbas-Seifried, M. Groessl, A. Egger, W. Berger, H. Zorbas, P. J. Dyson, B. K. Keppler, *Chem. Biodiversity* **2008**, *5*, 2140–2155.
[13] H. A. Burris, S. Bakewell, J. C. Bendell, J. Infante, S. F. Jones, D. R. Spigel, G. J. Weiss, R. K. Ramanathan, A. Ogden, D. Von Hoff, *ESMO Open* **2016**, *1*, e000154.
[14] A. Gandosio, K. Purkait, G. Gasser, *Chimia* **2021**, *75*, 845.
[15] D. Havrylyuk, A. C. Hachey, A. Fenton, D. K. Heidary, E. C. Glazer, *Nat. Commun.* **2022**, *13*, 3636.
[16] S. J. Steinke, S. Gupta, E. J. Piechota, C. E. Moore, J. J. Kodanko, C. Turro, *Chem. Sci.* **2022**, *13*, 1933–1945.
[17] G. He, N. Xu, H. Ge, Y. Lu, R. Wang, H. Wang, J. Du, J. Fan, W. Sun, X. Peng, *ACS Appl. Mater. Interfaces* **2021**, *13*, 19572–19580.
[18] S. Monro, K. L. Colón, H. Yin, J. Roque, P. Konda, S. Gujar, R. P. Thummel, L. Lilge, C. G. Cameron, S. A. McFarland, *Chem. Rev.* **2019**, *119*, 797–828.
[19] K. Eastham, P. A. Scattergood, D. Chu, R. Z. Boota, A. Soupart, F. Alary, I. M. Dixon, C. R. Rice, S. J. O. Hardman, P. I. P. Elliott, *Inorg. Chem.* **2022**, *61*, 19907–19924.
[20] A. Zamora, C. A. Denning, D. K. Heidary, E. Wachter, L. A. Nease, J. Ruiz, E. C. Glazer, *Dalton Trans.* **2017**, *46*, 2165–2173.
[21] D. Havrylyuk, K. Stevens, S. Parkin, E. C. Glazer, *Inorg. Chem.* **2020**, *59*, 1006–1013.
[22] N. Toupin, S. Steinke, S. Nadella, A. Li, T. Rohrabaugh, E. Samuels, C. Turro, I. Sevrioukova, J. Kodanko, *J. Am. Chem. Soc.* **2021**, *143*, 9191–9205.
[23] X. Guo, J. Qu, C. Zhu, W. Li, L. Luo, J. Yang, X. Yin, Q. Li, Y. Du, D. Chen, Y. Qiu, Y. Lou, J. You, *Drug Delivery* **2018**, *25*, 585–599.
[24] Z. Lv, H. Wei, Q. Li, X. Su, S. Liu, K. Y. Zhang, W. Lv, Q. Zhao, X. Li, W. Huang, *Chem. Sci.* **2018**, *9*, 502–512.
[25] Y. Sun, D. Zhao, G. Wang, Y. Wang, L. Cao, J. Sun, Q. Jiang, Z. He, *Acta Pharm. Sin. B* **2020**, *10*, 1382–1396.
[26] M. H. Al-Afyouni, T. N. Rohrabaugh, K. F. Al-Afyouni, C. Turro, *Chem. Sci.* **2018**, *9*, 6711–6720.

[27] G. S. Kulkarni, L. Lilge, M. Nesbitt, R. J. Dumoulin-White, A. Mandel, M. A. S. Jewett, *Eur. Urol. Open Sci.* **2022**, *41*, 105–111.
[28] Q. Chen, J.-A. Cuello-Garibo, L. Bretin, L. Zhang, V. Ramu, Y. Aydar, Y. Batsiun, S. Bronkhorst, Y. Husiev, N. Beztsinna, L. Chen, X.-Q. Zhou, C. Schmidt, I. Ott, M. J. Jager, A. M. Brouwer, B. E. Snaar-Jagalska, S. Bonnet, *Chem. Sci.* **2022**, *13*, 6899–6919.
[29] L. Zhang, P. Wang, X.-Q. Zhou, L. Bretin, X. Zeng, Y. Husiev, E. A. Polanco, G. Zhao, L. S. Wijaya, T. Biver, S. E. Le Dévédec, W. Sun, S. Bonnet, *J. Am. Chem. Soc.* **2023**, *145*, 14963–14980.
[30] G. Te Velde, F. M. Bickelhaupt, E. J. Baerends, C. Fonseca Guerra, S. J. A. Van Gisbergen, J. G. Snijders, T. Ziegler, *J. Comput. Chem.* **2001**, *22*, 931–967.
[31] M. Ernzerhof, G. E. Scuseria, *J. Chem. Phys.* **1999**, *110*, 5029–5036.
[32] E. Van Lenthe, E. J. Baerends, *J. Comput. Chem.* **2003**, *24*, 1142–1156.
[33] D. P. Chong, E. Van Lenthe, S. Van Gisbergen, E. J. Baerends, *J. Comput. Chem.* **2004**, *25*, 1030–1036.
[34] C. C. Pye, T. Ziegler, *Theor. Chem. Acc.* **1999**, *101*, 396–408.
[35] S. Grimme, S. Ehrlich, L. Goerigk, *J. Comput. Chem.* **2011**, *32*, 1456–1465.
[36] E. Van Lenthe, E. J. Baerends, J. G. Snijders, *J. Chem. Phys.* **1994**, *101*, 9783–9792.
[37] S. J. Steinke, E. J. Piechota, L. M. Loftus, C. Turro, *J. Am. Chem. Soc.* **2022**, *144*, 20177–20182.
[38] L. N. Lameijer, T. G. Brevé, V. H. S. van Rixel, S. H. C. Askes, M. A. Siegler, S. Bonnet, *Chem. Eur. J.* **2018**, *24*, 2709–2717.
[39] V. Vichai, K. Kirtikara, *Nat. Protoc.* **2006**, *1*, 1112–1116.
[40] L. M. Minassian, T. Cotechini, E. Huitema, C. H. Graham, in *Hypoxia Cancer Metastasis* (Ed.: D. M. Gilkes), Springer International Publishing, Cham, **2019**, pp. 123–139.
[41] X. Jing, F. Yang, C. Shao, K. Wei, M. Xie, H. Shen, Y. Shu, *Mol. Cancer* **2019**, *18*, 157.
[42] L. N. Lameijer, D. Ernst, S. L. Hopkins, M. S. Meijer, S. H. C. Askes, S. E. Le Dévédec, S. Bonnet, *Angew. Chem. Int. Ed.* **2017**, *56*, 11549–11553.
[43] X.-Q. Zhou, M. Xiao, V. Ramu, J. Hilgendorf, X. Li, P. Papadopoulou, M. A. Siegler, A. Kros, W. Sun, S. Bonnet, *J. Am. Chem. Soc.* **2020**, *142*, 10383–10399.

Manuscript received: October 30, 2023
Accepted manuscript online: December 7, 2023
Version of record online: ■■, ■■

Research Articles

Photopharmacology

L. Bretin, Y. Husiev, V. Ramu, L. Zhang, M. Hakkennes, S. Abyar, A. C. Johns, S. E. Le Dévédec, T. Betancourt, A. Kornienko, S. Bonnet* ___ **e202316425**

Red-Light Activation of a Microtubule Polymerization Inhibitor via Amide Functionalization of the Ruthenium Photocage

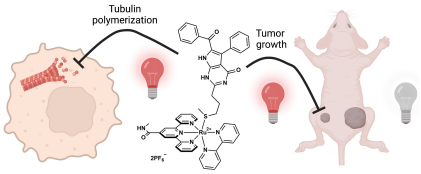

Methylamide functionalization of a green light-sensitive photoactivated chemotherapy agent based on ruthenium fine-tuned its excited states, dramatically improving red light absorption. The new prodrug inhibited microtubule polymerization under red light activation, efficiently killing cancer cells in vitro. In vivo, red light activation shrank non-melanoma skin tumors in mice, while in the dark the prodrug showed improved biosafety.